

Effects of Surface Step Density on the Electrochemical Oxidation of Ethanol to Acetic Acid

David J. Tarnowski[†] and Carol Korzeniewski*

Department of Chemistry and Biochemistry, Texas Tech University, Lubbock, Texas 79409-1061

Received: August 13, 1996; In Final Form: October 21, 1996[⊗]

The electrochemical oxidation of ethanol (0.3 M in 0.1 M HClO₄) was studied at Pt(111), Pt(557) ≡ Pt(s) – [6(111) × (100)], and Pt(335) ≡ Pt(s)–[4(111) × (100)] single crystal electrodes. The oxidation pathway leading to acetic acid showed a marked dependence on electrode surface structure; acetic acid formation decreased as the surface step density increased. On the stepped surfaces, facile C–C bond cleavage and high surface poisoning appear to account for the low acetic acid production. Isolation and quantification of acetic acid was achieved with ion chromatography. Oxidation products were generated in a small (~40 μL) drop of electrolyte solution in contact with a single crystal electrode and analyzed following a short (60 s) electrolysis period. This approach enabled the specific and quantitative determination of soluble reaction products. For Pt(111), results were compared with acetic acid yields determined by in-situ infrared spectroscopy. Agreement between the two methods is within the uncertainty of the techniques. The results support unanticipated findings of earlier infrared spectroscopy studies, which indicate ethanol oxidation to acetic acid is inhibited on platinum surfaces that contain high surface step densities. Additionally, the percent of charge due to acetic acid formation was obtained by comparing the total anodic charge passed with the moles of acetate detected.

Introduction

The electrochemical oxidation of ethanol has been studied primarily in support of fuel cell development. Ethanol has served both as a fuel¹ and as a mechanistic probe of organic oxidation reactions (cf. refs 2–4, and references cited therein). Similar to other small, oxygenated organic molecules,² the electrochemistry of ethanol is sensitive to the atomic-level electrode surface structure.^{5–11} This dependency appears to arise from a competition between chemical bond activation and electrode poisoning, both of which are affected by electrode surface atom coordination (cf. ref 10).

Electrochemical reactions of ethanol have been studied most extensively with platinum electrodes. At single crystal platinum, cyclic voltammetry experiments show marked differences in the response to ethanol oxidation among the low index surface planes.^{5–8,10} On a positive-going sweep starting from the hydrogen adsorption region, anodic current densities during the first half of the sweep are greater at Pt(111) than at other platinum surfaces. For analogous sweeps in acid electrolytes, the current density peaks about 200 mV less positive for Pt(111) than for Pt(100) and Pt(110). Differences have been linked to the ability of the surfaces to support the formation and adsorption of carbon monoxide (CO) and other partial oxidation products.^{5–10}

Molecular level studies of ethanol oxidation on single crystal platinum electrodes have mainly employed infrared spectroscopy.^{9–11} Reactions in aqueous acid electrolytes have been investigated. Acetaldehyde (CH₃CHO), acetic acid, and carbon dioxide appear as major soluble products, while CO is the most commonly detected adsorbate. Ethoxy and acetyl adsorbates have also been observed at polycrystalline platinum electrodes.^{3,12,13} Infrared spectroscopy has shown that CO coverages are lower on Pt(111) than on other platinum

electrodes.^{9–11} Surfaces with low coordination sites, such as Pt(110) and polycrystalline platinum, appear to activate ethanol C–C bond cleavage and produce more adsorbed CO.^{10,11} Pathways that lead to acetaldehyde and acetic acid also show a dependence on electrode surface structure. Following the removal of chemisorbed poisons, infrared spectra indicate that acetic acid forms almost exclusively in reactions at Pt(111) but that nearly equal amounts of acetic acid and acetaldehyde form at Pt(110) and Pt(100).¹⁰

The present study further investigates the effects of electrode surface structure on ethanol oxidation pathways in experiments with Pt(111), Pt(557) ≡ Pt(s) – [6(111) × (100)], and Pt(335) ≡ Pt(s) – [4(111) × (100)] electrodes. Effects of surface step density on acetic acid formation are probed. In contrast to infrared spectroscopy, which can be limited in the determination of soluble species by the thin layer electrochemical cell geometry,^{14–19} acetic acid produced from ethanol oxidation is determined more specifically and quantitatively with the use of ion chromatography.²⁰ Experiments show that acetic acid formation is greatest on Pt(111) and decreases with increasing surface step density over the range of 0.2–0.6 V (vs SCE) during positive-going potential excursions. These results support earlier, unexpected findings which indicate the four-electron oxidation pathway to acetic acid is inhibited on surfaces with a high density of low coordination sites.^{9,10} Comparison of the moles of acetic acid formed and the charge consumed during electrolysis indicates that at Pt(111) as much as 30% of the oxidative charge is due to acetic acid formation.

Experimental Section

Reagents. All solutions were made with 18 MΩ water from a four-cartridge nanopure system (Barnstead, Des Moines, IA). Perchloric acid (Aldrich, Milwaukee, WI; 99.999% purity), glacial acetic acid (Aldrich), Na₂B₄O₇ (Aldrich), methylene chloride (EM, Gibbstown, NJ), ethanol (Aaper, Shelbyville, KY), and compressed oxygen (Big Three, Houston, TX) were of reagent grade or better and were used as received. Hydrogen (Liquid Carbonic, Oak Brook, IL) and argon (Trinity Gases, Dallas, TX) were of ultrahigh purity.

* Author to whom correspondence should be addressed. E-mail address: BFKOR@ttacs.ttu.edu.

[†] Permanent address: Department of Chemistry, University of Michigan, Ann Arbor, MI 48109.

[⊗] Abstract published in *Advance ACS Abstracts*, December 15, 1996.

Pt Single Crystal Electrode Preparation. For the preparation of platinum electrodes, the methods in refs 21–23 were followed. One end of about 3 cm of Pt wire (Johnson Matthey; puratronic grade, 1 mm diameter) was held with a tweezers attached to a ring stand and heated in a H_2/O_2 flame until a molten bead (~ 3 mm diameter) formed at the free end. The melt zone, observed through glass blower's goggles or suitable neutral density filters, was slowly moved up and down by adjusting the proximity of the flame to the bottom of the bead. Larger electrodes (~ 4 mm diameter) were formed by adding small amounts of Pt (99.95%) to the base of a bead and melting further. After about 30 melting and cooling cycles, symmetrically positioned facets (~ 0.3 mm diameter) appeared around the Pt surface. Following facet formation, a bead was secured to a two axis goniometer (South Bay Technologies, San Clemente, CA, Model 250) and oriented by laser back-reflection.^{22,23} A He/Ne laser (Uniphase, Manteca, CA; 0.95 mW) was mounted on a y - z translation stage at one end of an optical table and positioned with the beam axis parallel to an optical rail (Oriel). The goniometer was attached to a translation stage (South Bay, Model 25002) and positioned on the optical rail at a laser-to-bead distance of 1.5 m. Crystals were secured for optical alignment by first setting the wire extending from the base of a bead into casting wax (Kerr, Emeryville, CA) inside a plastic ring affixed to the goniometer. After initial orientation, small amounts of acrylic resin (Buehler, Lake Bluff, IL, Ultramount) were placed around the crystal stepwise, leaving facets of interest exposed. Crystal alignment was checked after each addition of resin in order to correct for small changes in position due to resin contraction on hardening. Crystals were oriented by adjusting the goniometer so that light incident on a facet was reflected back along the optical axis of the laser and onto a screen surrounding the laser aperture. Facets of (111) and (100) served as guideposts for crystal alignment. Reflections from (111) facets were brighter and sharper than reflections from (100) facets. Adjacent (111) and (100) facets produced reflection spots with an angular separation of 54.7° , as predicted.²⁴ Higher index planes were obtained by first orienting on a (111) reflection spot and then tilting toward a (100) reflection spot. Tilt angles of 14.42° and 9.45° from a Pt(111) reflection correspond to Pt(335) and Pt(557) orientations, respectively.²⁴ Once the entire bead was covered with acrylic resin, the goniometer, with a properly oriented crystal, was mounted on a lapping fixture (South Bay, Model 25010). Crystal faces were exposed and polished to a mirrorlike finish with successively finer grades of abrasive paper (Buehler, 320, 400, and 600 grit) and alumina (Buehler, $9.5 \mu\text{m}$ to $0.05 \mu\text{m}$) on a rotating wheel polisher (Buehler, Ecomet IV). Polishing debris was removed between each grade of abrasive by ultrasonic cleaning. After the acrylic resin was dissolved with methylene chloride, the orientation of a polished crystal face of an electrode was checked by Laue X-ray diffraction^{24,25} to an accuracy of better than 0.5° .

Electrochemistry. Before each experiment, Pt single crystal electrodes were polished with $0.05 \mu\text{m}$ alumina and cleaned by sonication. Electrodes were annealed for ~ 5 min in a H_2 flame and cooled in a stream of Ar above Ar saturated water. When no longer red, electrodes were quenched in the water and then transferred, with a drop of water hanging from the electrode to prevent surface disordering by the atmosphere, to an electrochemical cell. Surface cleanliness and order were verified by cyclic voltammetry prior to each experiment. Waves characteristic of each surface were observed for potential sweeps at 50 mV/s in 0.1 M HClO_4 .

Electrochemical cell potentials were maintained with a three electrode potentiostat (PAR Model 273/86, Princeton, NJ)

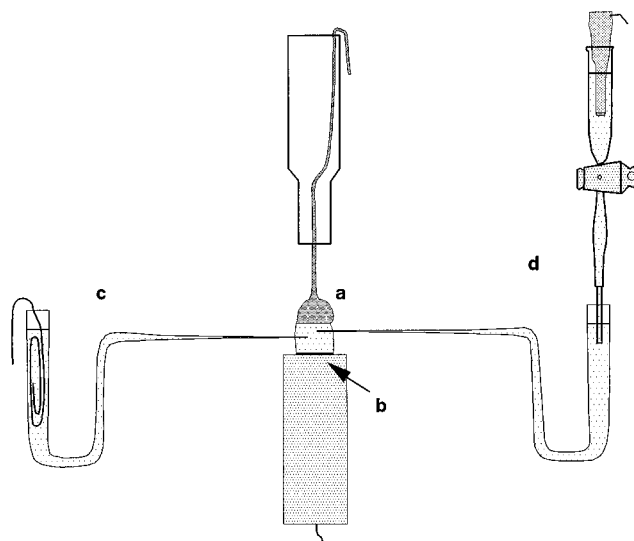


Figure 1. Diagram of experimental apparatus used for sample electrolysis. The Pt single crystal electrode (a) contacts a drop ($\sim 40 \mu\text{L}$) of sample solution on top of a shrouded Pt disk (b) (the Pt disk served as the counter electrode in initial experiments). The counter and reference electrodes (c and d, respectively) mount in separate compartments and contact the sample solution through narrow, electrolyte-filled glass capillaries. (Not drawn to scale).

controlled though an IEEE-488 interface bus by a microcomputer running Model 270/250 Research Electrochemistry Software (PAR), version 4.00. Cyclic voltammetry experiments with ethanol were recorded in a three-electrode electrochemical cell with a Pt wire counter electrode and a saturated calomel reference electrode (SCE). The reference electrode was located in an external compartment that connected to the sample solution through a wetted stopcock and a Luggin capillary. Single crystal electrodes (ca. 0.071 cm^2) were positioned to form a reverse meniscus with the test solution. Following a background scan in 0.1 M HClO_4 , the potential was held at -0.24 V and ethanol was added to the desired concentration. The solution was gently mixed with a syringe for $\sim 30 \text{ s}$, after which two cyclic scans were recorded at 50 mV/s between -0.24 and $+0.64 \text{ V}$. All potentials are reported vs SCE.

Ethanol electrolysis experiments utilized larger (ca. 0.12 cm^2) single crystal Pt bead electrodes in approximately $40 \mu\text{L}$ of air-saturated solution (see Figure 1). After quenching, electrodes were transferred with a hanging drop of water ($\sim 10 \mu\text{L}$) and placed into contact with $15 \mu\text{L}$ of 0.1 M HClO_4 located on top of a Teflon shrouded 0.125 cm^2 Pt disk (Figure 1b) (Pine Instrument Co., Grove City, PA, Model No. AFVD0480). In initial experiments, the Pt disk was used as the counter electrode but was later replaced by a Pt wire held in a separate compartment (Figure 1c). A SCE located behind a wetted stopcock (Figure 1d) was connected to the sample solution through a soft glass capillary. With potential control established at -0.24 V , $15 \mu\text{L}$ of 0.75 M ethanol in 0.1 M HClO_4 was added to the test solution, bringing the total volume to $\sim 40 \mu\text{L}$. After an approximately 10 s equilibration period, the electrode was stepped to a constant potential between 0.2 and 0.6 V for 60 s . At the end of the electrolysis period, all capillaries were removed from the drop and $30 \mu\text{L}$ of sample was withdrawn and diluted in 1.0 mL of ultrapure water. Current transients for each experiment were stored for future use.

Chromatographic Determination of Acetate. Diluted samples were injected ($25 \mu\text{L}$) into an ion chromatograph (Dionex, DX100, Sunnyvale, CA) immediately after ethanol electrolysis. All components, including columns, injection

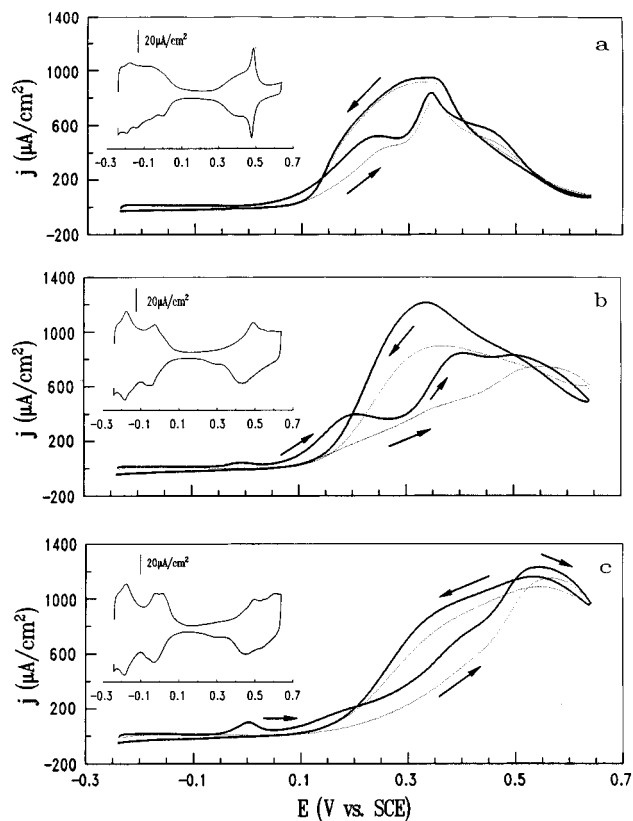


Figure 2. Cyclic voltammograms of ethanol (0.3 M in argon-saturated 0.1 M HClO₄) recorded with Pt(111), Pt(557), and Pt(335) electrodes (a–c, respectively). Ethanol was added to the cells with the electrodes poised at -0.24 V (vs SCE). Scans were started ~ 30 s after addition of ethanol. The first (solid lines) and second (dashed lines) cyclic scans are displayed. Insets show cyclic voltammograms recorded in 0.1 M HClO₄ prior to addition of ethanol to the solution. All voltammograms were recorded at a scan rate of 50 mV/s. Arrows indicate scan directions.

valve, conductivity detector, and suppressor, were from Dionex. The eluent, 10 mM Na₂B₄O₇, was pumped at 2.0 mL/min. Separations were performed on a AS4A-SC (4 mm) analytical column, used in combination with an AG4A-SC guard column (4 mm). A conductivity detector with an electrically operated autosuppressor (ASRS-I; 4 mm) were used for detection. Deionized water was used as the regenerant. Acetate calibration curves were recorded with freshly prepared standards and run immediately after sample analysis.

Results

Figure 2 shows cyclic voltammograms recorded with Pt(111), Pt(557), and Pt(335) electrodes before and after the addition of ethanol to 0.1 M HClO₄. On initial sweeps in ethanolic solutions, the current is negligible at all electrodes between -0.25 and $+0.05$ V (vs SCE), except for a weak anodic wave at ~ 0.0 V for Pt(557) and Pt(335). The anodic peak is roughly coincident with the hydrogen desorption feature present in the voltammograms of Pt(557) and Pt(335) in blank electrolyte (Figure 2b,c, insets). The peak current for this wave increases with increasing surface step density.

Between 0.05 and 0.65 V (vs SCE) on the forward sweeps, broad anodic features associated with ethanol oxidation^{5–8,10} appear on all surfaces. As noted previously,^{7,8} the voltammetric response across this range is characterized by three waves. The current density in the first two waves, in the regions 0.05–0.3 and 0.3–0.5 V, respectively, is greatest at Pt(111) and decreases with increasing surface step density. The current at Pt(111)

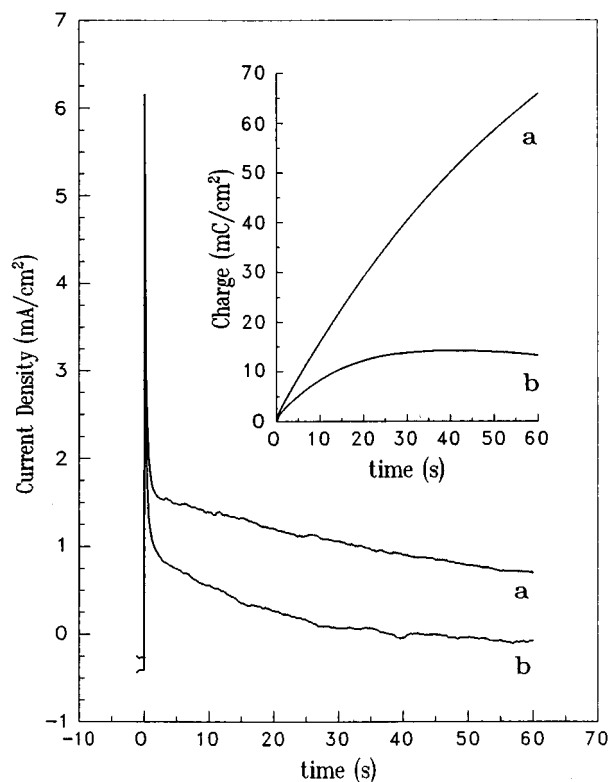


Figure 3. Chronoamperometry of ethanol (0.3 M in 0.1 M HClO₄) at Pt(111) (a) and Pt(335) (b) electrodes recorded using the experimental configuration shown in Figure 1. Ethanol was added to the drop with the working electrode potential held at -0.24 V, and the potential was stepped to $+0.3$ V after a short (~ 3 s) equilibration. Inset shows the corresponding charge vs time traces.

reaches a maximum between 0.3 and 0.5 V, while the current density at Pt(557) and Pt(335) increases continuously across this region. The third wave, between 0.5 and 0.65 V, attains the largest current density at Pt(335) and decreases in the order Pt(335) > Pt(557) > Pt(111).

Return sweeps display broad anodic waves. The current density at Pt(111) and Pt(557) increases from 0.6 to 0.3 V. The anodic wave at Pt(335) peaks at about 0.5 V and then slowly decays until the potential reaches 0.3 V. The current density decreases sharply for all surfaces on the return sweep between 0.1 and 0.2 V. The decline is steeper and the current returns to base line at more positive potentials for the stepped surfaces than those for Pt(111). Second scans show a slight decrease in activity compared to the initial sweeps, consistent with previous measurements.⁶

In ion chromatography experiments, acetic acid formed following a step from -0.24 V to more positive potentials was determined. Samples were generated by electrolysis using the experimental setup shown in Figure 1. The small volume allowed detectable quantities of reaction products to be formed with the necessarily small single crystal electrodes in relatively short (60 s) electrolysis times. In initial experiments, cyclic voltammograms were recorded to ensure consistency with the response in the conventional three-electrode cell. Voltammograms obtained with ethanol in the liquid drop were identical to those in Figure 2, except for a slight negative current offset due to oxygen reduction in the air-saturated drop.

Figure 3 shows current transients recorded during a potential step from -0.24 to $+0.3$ V at Pt(111) and Pt(335) electrodes in electrolyte containing approximately 0.3 M ethanol. Both transients display appreciable current during the early stages of oxidation. The transient for ethanol oxidation at Pt(335) dips below zero current near the end of the time period, due to effects

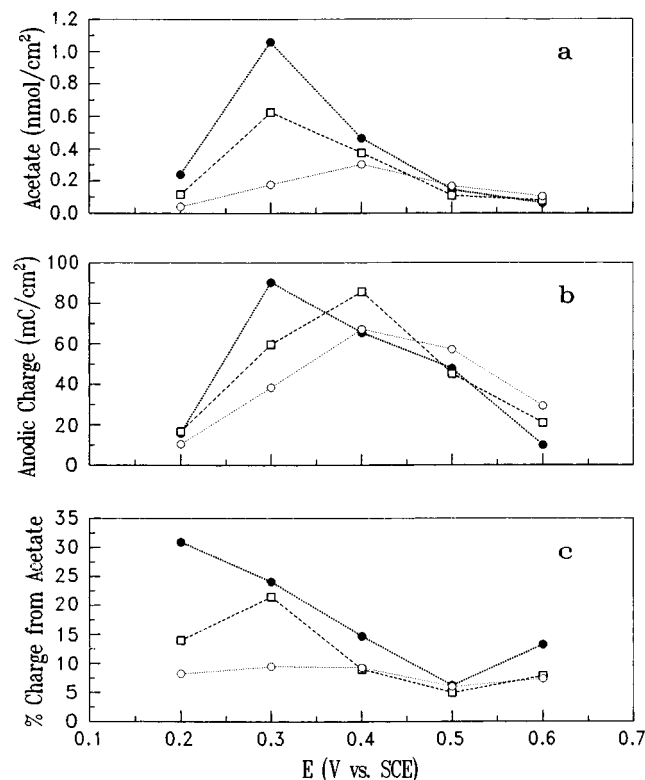


Figure 4. Plots showing the quantity of acetate formed (a), the anodic charge passed (Q_{anodic}) (b), and the percentage of charge due to acetate formation (c) as a function of potential at Pt(111) (●), Pt(557) (□), and Pt(335) (○) electrodes.

of oxygen reduction (vide infra). The response for Pt(557) (not shown) was intermediate between that for Pt(111) and Pt(335). The current measured during electrolysis at 0.3 V increases with decreasing step density, analogous to the current at this potential in the cyclic voltammograms (Figure 2). The charge obtained from digital integration of the current transients is shown as an inset to Figure 3.

Electrolysis experiments were run for each electrode poised at potentials from 0.2 to 0.6 V. At the end of each 60 s electrolysis period, samples were diluted and analyzed by ion chromatography. One major peak appeared in all chromatograms, assignable to acetate formed from acetic acid. Smaller peaks assignable to carbonate and trace chloride were also detected. Chloride, present at about 4×10^{-7} M, likely originated from the reference capillary. Carbonate is believed to arise in part from CO_2 generated during ethanol oxidation but was not quantifiable due to the background presence of carbonate from atmospheric CO_2 . Injection of standards containing both acetate and formate showed that the two analytes were well-resolved under the present experimental conditions. Formate was not detected in electrolysis products. (The 10 mM borate buffer did not elute perchlorate from the column. Non-eluting ions were removed from the column at the end of each day with 50 mM borate buffer.)

The quantity of acetic acid detected in each experiment is summarized in Figure 4a. On Pt(111) and Pt(557), the acetate amounts reach a maximum at 0.3 V and fall off at more positive potentials. The response at Pt(335) is similar, except that the maximum occurs at a slightly more positive potential, +0.4 V. For electrode potentials ≤ 0.4 V, the acetic acid yield is greatest at Pt(111) and decreases as the surface step density increases. These results confirm that there is a greater preference for the direct oxidation of ethanol to acetic acid on atomically smooth platinum than on stepped platinum surfaces.^{9,10}

TABLE 1: Acetic Acid Detected from 60 s Ethanol Electrolysis

electrolysis potential (V vs SCE)	charge due to acetic acid formation ^a (mC/cm^2)		
	Pt(111)	Pt(557)	Pt(335)
0.2	4.92	2.40	0.86
0.3	21.8	12.9	3.64
0.4	9.59	7.71	6.23
0.5	2.95	2.23	3.43
0.6	1.30	1.63	2.14

^a From eq 2.

The quantity of acetic acid produced at each electrode was compared to the total anodic charge generated during electrolysis (Q_{anodic}). Q_{anodic} was calculated from

$$Q_{\text{anodic}} = Q_{\text{total}} - Q_{\text{red}} \quad (1)$$

where Q_{total} is the charge obtained from integration of current transients recorded during ethanol oxidation and Q_{red} is the charge due to oxygen reduction, determined from current transients measured in blank electrolyte. Over the potential range studied, Q_{anodic} values determined with eq 1 agreed well with values of Q_{total} measured during ethanol oxidation in a conventional three-electrode cell under oxygen free conditions (i.e., when $Q_{\text{red}} \approx 0$). At potentials below 0.2 V, this approach proved to overcompensate for the effects of oxygen reduction, presumably due to surface poisoning at low potentials, which deactivates sites for oxygen reduction in ethanol solutions.

Plots of anodic charge recorded during ethanol oxidation at Pt(111), Pt(557), and Pt(335) electrodes are shown in Figure 4b. At potentials ≤ 0.4 V, the charge recorded in experiments with Pt(111) tracks the corresponding curve for the quantity of acetic acid generated (Figure 4a, filled circles). For Pt(557) and Pt(335), the charges over this potential region reach a maximum at about 0.4 V and do not correlate closely with acetic acid production. The response indicates that other species, such as acetaldehyde and CO_2 , are generated as primary products at the stepped surfaces.

At potentials more positive than 0.4 V, the anodic charge displayed in Figure 4b decreases for all surfaces. For Pt(557) and Pt(335), this response appears to conflict with the cyclic voltammetry (Figure 2b,c), where the current increases above 0.4 V. However, in the cyclic voltammetry, the oxidation processes at high potentials are associated mainly with adsorbed species (c.f. ref 5), which are not replenished at high potentials. In addition, fewer adsorbates may form in a step experiment because adsorption processes that occur at intermediate potentials may be bypassed.

Figure 4c shows the percentage of Q_{anodic} that arises from acetate formation at different potentials. The charge consumed during acetic acid production was determined from the moles of acetic acid detected, assuming the four electron oxidation pathway



The charge due to acetic acid formed at different potentials in experiments with the single crystal electrodes is reported in Table 1. Acetic acid formation consumes a larger fraction of charge in reactions on Pt(111) than on the stepped Pt surfaces. As step density increases, other processes account for anodic charge, most likely pathways leading to acetaldehyde and CO_2 , as discussed earlier.

Discussion

The electrochemical and chromatographic experiments demonstrate effects of surface structure on ethanol oxidation at

platinum electrodes. The decrease in acetic acid production with an increase in surface step density coincides with trends observed in infrared spectroscopy experiments.^{9,10} During a potential sweep from -0.25 to $+0.6$ V (vs. SCE), vibrational bands for acetic acid appeared at less positive potentials on Pt(111) than on other platinum surfaces. In these spectroscopic studies, acetic acid formation was blocked at Pt(110), Pt(100), and polycrystalline platinum electrodes at potentials below about 0.4 V, and the two electron oxidation product acetaldehyde appeared dominant.^{9,10} This inhibition in the acetic acid producing pathway at stepped platinum electrodes (Pt(100) electrodes have been shown to restructure in aqueous solution, forming nanoscopic domains with high step site coverages²⁶) coincides with the decrease in acetic acid formation at Pt(557) and Pt(335) electrodes indicated in Figure 4a.

The chromatography results are also consistent with product distributions from ethanol oxidation determined with the use of in-situ mass spectrometry. Acetaldehyde was determined to be the main two carbon oxidation product in reactions at polycrystalline platinum,^{27,28} platinum black,¹ and platinum–ruthenium¹ electrodes, which have a high density of low coordination sites. Acetic acid has not been detected as a product of ethanol oxidation in in-situ mass spectrometry studies, which thus far appear restricted to polycrystalline and Pt(110) electrodes.^{1,3,4,27,28}

The surface structure sensitivity of ethanol oxidation is due in part to facile C–C bond cleavage at step sites.¹¹ The faster C–C bond breaking kinetics lead to larger CO₂ yields^{9–11} but at the expense of increased poisoning by adsorbed CO^{9–11} and possibly other partial oxidation products.^{3,4,12,13,28} The decrease in acetic acid production with increased surface step density is likely a consequence of (i) a shift in reactions toward the CO₂ producing pathway and (ii) increased surface poisoning that blocks sites for water activation (eq 2).^{9,10} The latter can account for the preferential formation of acetaldehyde on partially blocked stepped surfaces.^{9,10}

The chromatographic experiments also provide a check on the quantitative capabilities of the thin layer infrared spectroscopy technique. Infrared spectroelectrochemistry has many virtues, especially in the detection of adsorbates;^{18,29} however, the thin layer cell geometry can limit accuracy in the quantification of soluble species. Electric field inhomogeneity in the thin layer cavity,^{14–16,18,19} product leakage,¹⁰ reactant depletion,^{10,17} and nonuniform cavity thickness¹⁷ can affect the intensity of vibrational bands and lead to errors in quantitative measurements.¹⁶ Also, in the study of ethanol oxidation, the carbonyl stretching bands for acetaldehyde and acetic acid overlap, and independent determinations require extending the infrared spectral window below 1000 cm⁻¹.^{9,10} Ion chromatography allows the soluble products to be determined more specifically (vide infra) and quantitatively.

Figure 4a can be compared to the plots of acetic acid quantity vs potential, generated from in-situ infrared spectra.^{9,10} The curve for Pt(111) in Figure 4a corresponds to the traces for acetic acid in Figure 9 of ref 10 and Figure 3 of ref 9. The curve in Figure 4a is proportional to the *derivative* of the plots generated from infrared spectra. Since infrared spectra were collected during a slow potential sweep, products accumulate in the thin layer cavity through the duration of the scan. In contrast, samples for chromatography were obtained following a single potential step and are not affected by the buildup of products generated at intermediate potentials. Data from Figure 4a and infrared spectroscopy show excellent correspondence. Both indicate the rate of acetic acid generation maximizes between 0.3 and 0.4 V and then quickly falls off for potentials ≤ 0.4 V.

The absolute amounts of acetic acid detected by each technique can also be compared. Over the potential range between 0.25 and 0.35 V, infrared spectroscopy determinations indicate that 2–3 nmol of acetic acid are generated during a 2 mV/s sweep (50 s measurement period).^{9,10} Figure 4a shows that 1.2 nmol of acetic acid are produced during a 60 s measurement period at 0.3 V. Agreement between the two methods is within a factor of 2, which approaches the uncertainty in the electromagnetic enhancement (ref 9, p 323) in the thin layer cavity.^{9,10} Currently, the protocol used in chromatographic determination of electrochemically generated acetic acid is limited by uncertainty in the solution volume of the drop that protects the single crystal electrode during transfer to the electrolyte. With more accurate measurement of drop volumes, the chromatographic technique can provide a means for calibration in quantitative infrared spectroelectrochemical experiments.

The conditions employed in the present study did not allow for detection of acetaldehyde and carbon dioxide, which are also major reaction products. Strategies for determination of aldehydes, through reaction with phenylhydrazine compounds,³⁰ are under investigation. In addition, it should be noted that acetaldehyde can oxidize to acetic acid in the presence of atmospheric oxygen.^{31–33} Our studies of this side reaction have indicated that it is slow and does not significantly affect the acetic acid determinations under the present experimental conditions.

Conclusions

The ethanol oxidation pathway leading to the formation of acetic acid is markedly affected by the electrode atomic-level surface structure. The quantity of acetic acid produced during positive potential sweeps is greatest across the range 0.2–0.6 V and decreases with increasing surface step density. Studies show that soluble products of reactions at single crystal electrodes can be isolated and quantified with the use of ion chromatography. In the determination of soluble species, the chromatographic technique can overcome limitations of in-situ infrared spectroscopy and provide a means for calibration in infrared experiments.

Acknowledgment. We are grateful for the assistance of Dr. G. M. Swain (Utah State University) during the fabrication of single crystal electrodes, Dr. N. Güven and V. Polyak with X-ray backscattering measurements, and Drs. C. E. Evans (University of Michigan), P. K. Dasgupta, and A. Sjögren with preliminary ion chromatography experiments. We also appreciate the assistance of Mr. J. Serafini with acetaldehyde stability studies. Financial support for this work was provided by the U.S. Office of Naval Research.

References and Notes

- (1) Wang, J.; Wasmus, S.; Savinell, R. F. *J. Electrochem. Soc.* **1995**, *142*, 4218.
- (2) Beden, B.; Leger, J.-M.; Lamy, C. In *Modern Aspects of Electrochemistry*; Bockris, J. O'M., Conway B. E., White, R. E., Eds.; Plenum: New York, 1992; Vol. 22, p 97.
- (3) Iwasita, T.; Pastor, E. *Electrochim. Acta* **1994**, *39*, 531.
- (4) Schmiemann, U.; Muller, U.; Baltruschat, H. *Electrochim. Acta* **1995**, *40*, 99.
- (5) Cases, F.; Lopez-Atalaya, M.; Vazquez, J. L.; Aldaz, A.; Clavilier, J. *J. Electroanal. Chem.* **1990**, *278*, 433.
- (6) Morin, M.-C.; Lamy, C.; Leger, J.-M.; Vasquez, J.-L.; Aldaz, A. *J. Electroanal. Chem.* **1990**, *283*, 287.
- (7) Cases, F.; Vazquez, J.-L.; Perez, J. M.; Aldaz, A. *J. Electroanal. Chem.* **1991**, *310*, 403.
- (8) Cases, F.; Morallon, E.; Vazquez, J.-L.; Perez, J. M.; Aldaz, A. *J. Electroanal. Chem.* **1993**, *350*, 267.
- (9) Leung, L. W. H.; Chang, S. C.; Weaver, M. J. *J. Electroanal. Chem.* **1989**, *266*, 317.

- (10) Chang, S. C.; Leung, L. W. H.; Weaver, M. J. *J. Phys. Chem.* **1990**, *94*, 6013.
- (11) Shin, J.; Tornquist, W. J.; Korzeniewski, C.; Hoaglund, C. S. *Surf. Sci.* **1996**, *364*, 122.
- (12) Beden, B.; Morin, M. C.; Hahn, F.; Lamy, C. *J. Electroanal. Chem.* **1987**, *229*, 353.
- (13) Holze, R. *J. Electroanal. Chem.* **1988**, *246*, 449.
- (14) Seki, H.; Kunimatsu, K.; Golden, W. G. *Appl. Spectrosc.* **1985**, *39*, 437.
- (15) Popenoe, D. D.; Stole, S. M.; Porter, M. D. *Appl. Spectrosc.* **1992**, *46*, 79.
- (16) Leung, L. W. H.; Weaver, M. J. *J. Phys. Chem.* **1988**, *92*, 4019.
- (17) Corrigan, D. S.; Weaver, M. J. *J. Electroanal. Chem.* **1988**, *241*, 143.
- (18) Korzeniewski, C.; Severson, M. W. *Spectrochim. Acta* **1995**, *51A*, 499.
- (19) Faguy, P. W.; Marinkovic, N. S. *Anal. Chem.* **1995**, *67*, 2791.
- (20) Dasgupta, P. K. *Anal. Chem.* **1992**, *64*, 775A.
- (21) Clavilier, J.; Faure, R.; Guinet, G.; Durand, R. *J. Electroanal. Chem.* **1980**, *107*, 205.
- (22) Clavilier, J.; Armand, D.; Sun, S. G.; Petit, M. *J. Electroanal. Chem.* **1986**, *205*, 267.
- (23) Clavilier, J.; Achi, K. E.; Rodes, A. *Chem. Phys.* **1990**, *141*, 1.
- (24) Barrett, C. S. *Structure of Metals*; McGraw-Hill: New York, 1966.
- (25) Wood, E. A. *Crystal Orientation Manual*; Columbia University Press: New York, 1963.
- (26) Villegas, I.; Weaver, M. J. *J. Electroanal. Chem.* **1994**, *373*, 245.
- (27) Willsau, J.; Heitbaum, J. *J. Electroanal. Chem.* **1985**, *194*, 27.
- (28) Bittins-Cattaneo, B.; Wilelm, S.; Cattaneo, E.; Buschmann, H. W.; Vielstich, W. *Ber. Bunsen-Ges. Phys. Chem.* **1988**, *92*, 1210.
- (29) Chang, S. C.; Weaver, M. J. *J. Phys. Chem.* **1991**, *95*, 5391.
- (30) Dasgupta, P. K.; Zhang, G.; Schulze, S.; Marx, J. N. *Anal. Chem.* **1994**, *66*, 1965.
- (31) Larkin, D. R. *J. Org. Chem.* **1990**, *55*, 1563.
- (32) Bawn, C. E. H.; Williamson, J. B. *Trans. Faraday Soc.* **1951**, *47*, 721.
- (33) Sajus, L.; de Roch, I. S. In *Comprehensive Chemical Kinetics*; Bamford, C. H., Tipper, C. F. H., Eds.; Elsevier: Amsterdam, 1980; Vol. 16, p 88.